The Knee 63 (2026) 104604

Contents lists available at ScienceDirect

The Knee

journal homepage: www.elsevier.com/locate/thekne

Influence of enzymatic degeneration and mechanical damage on cartilage tissue mechanics: an in vitro biomechanical study

Asif Istiak [a], Ahmed Suparno Bahar Moni [b], Tanvir R. Faisal [a,*]

[a] Department of Mechanical Engineering, University of Louisiana at Lafayette, LA 70503, USA
[b] Department of Orthopedic Surgery, College of Medicine and Life Sciences, University of Toledo, OH 43614, USA

ARTICLE INFO

Article history:
Received 24 March 2026
Revised 2 July 2026
Accepted 5 August 2026
Available online xxxx

Keywords:
Articular cartilage
Focal cartilage defect
MMP
ADAMTS
Biomechanics

ABSTRACT

Background: Articular cartilage degeneration arising from the complex interplay of focal defect and enzymatic degradation compromises its morpho-mechanical integrity. The lack of comprehensive characterization of this combined pathology limits our mechanistic understanding of osteoarthritis (OA) initiation and progression.

Methods: Cylindrical osteochondral explants were harvested from six bovine knee joints and allocated into five experimental groups (n = 12 per group): intact healthy cartilage (Control), focal defect alone (Def), enzymatic degradation alone (Enz), enzymatic degradation followed by focal defect (Enz+Def), and focal defect followed by enzymatic degradation (Def+Enz). *In vitro* mechanical characterization was performed under three loading configurations—ramp compression, multi-step stress-relaxation, and dynamic sinusoidal loading conditions—to characterize the elastic and viscoelastic properties of each group. Semi-quantitative compositional and histological analyses were conducted using Fourier transform infrared (FTIR) spectroscopy, light, and polarized light microscopy.

Results: Enzymatic degradation plays a dominant role in compromising cartilage mechanical integrity, with enzymatically degraded cartilage exhibiting substantially greater mechanical deterioration than cartilage with a focal defect alone. FTIR analysis revealed greater zone-wise collagen loss than proteoglycan depletion in Enz group. While the combined insults compromised mechanical response across all loading conditions, Enz+Def group produced the most severe reduction in compressive (79.7% ($p < 0.001$, 95% CI : $[58.1\%, 90.1\%]$)) and equilibrium (97.7% ($p < 0.001$, $[95.1\%, 98.9\%]$)) moduli and dynamic loading capacity relative to Control.

Conclusion: To the best of our knowledge, this is the first study to systematically combine and sequence enzymatic degradation and a focal cartilage defect, providing mechanistic insight into their isolated and combined effects on cartilage morpho-mechanics with relevance to OA pathomechanics and early intervention strategies.

* Corresponding author at: Department of Mechanical Engineering, 241 E Lewis St., University of Louisiana at Lafayette, Lafayette, LA 70503, USA.
E-mail addresses: asif.istiak1@louisiana.edu (A. Istiak), AhmedSuparno.BaharMoni@UToledo.Edu (A.S. Bahar Moni), tanvir.faisal@louisiana.edu (T.R. Faisal).

https://doi.org/10.1016/j.knee.2026.104604

1. Introduction

The mechanical behavior of articular cartilage is fundamentally governed by the composition and structural organization of its extracellular matrix (ECM), primarily type II collagen fibrils and proteoglycans (PGs). Cartilage damage compromises load-bearing capacity through two concurrent mechanisms: disruption of the collagen fibrillar network—responsible for the tissue's tensile and elastic integrity [1] and breakdown of the PG constituents that confer compressive strength and viscoelastic capacity [2]. Focal cartilage damage further establishes a pro-inflammatory microenvironment in which catabolic enzymes are upregulated, including matrix metalloproteinases (MMPs), aggrecanases—a disintegrin and metalloproteinase with thrombospondin motifs (ADAMTS), and cathepsins, collectively driving enzymatic degradation of the ECM [3]. While both enzymatic degradation and mechanical damage are individually detrimental to cartilage health, their isolated and combined effects on cartilage mechanics remain insufficiently characterized, limiting our understanding of the initiation and progression of osteoarthritis (OA).

Mechanical damage to articular cartilage can originate from obesity, injurious overloading, repeated mechanical loading, axial knee malalignment, meniscectomy, patellar dislocation, and osteochondritis dissecans [4–8]. Structural damage including focal cartilage defects, fissures, tears, and cracks in the cartilage is predominantly observed in 60–66% of patients undergoing knee arthroscopy; however, 43% to 58% of articular cartilage defects occur on the load-bearing femoral condyle [9,10]. According to the International Cartilage Repair Society (ICRS) classification, full thickness fissures extending to the subchondral bone (Grade III) typically require surgical intervention [11,12]. The size of cartilage lesions varies widely, ranging from under 2 cm^2 to over 8 cm^2 depending on anatomical locations and patient-specific clinical factors [4]. While not all focal defects progress to OA, such lesions represent a recognized contributing factor in knee OA development and can accelerate disease progression by altering joint contact mechanics and stress distribution. Understanding how focal defects alter the intrinsic mechanical properties of cartilage tissue is therefore essential to elucidating the pathomechanical basis of OA initiation and progression.

Among the catabolic mediators implicated in cartilage degeneration, MMPs and ADAMTS family enzymes are the principal drivers of ECM breakdown, targeting the two primary structural constituents—collagen and PGs. Overexpressed MMPs in osteoarthritic cartilage drive irreversible collagen degradation through a sequential two-step cascade: collagenases (MMP-1, −8, −13) first cleave native collagen fibrils at specific triple-helical sites, after which gelatinases (MMP-2, −9) degrade the resulting denatured collagen fragments [13]. In this study, MMP-13 (collagenase-3) was selected as the representative collagenolytic agent, given its role as the principal collagenolytic effector in OA, and its high substrate specificity and catalytic efficiency for type II collagen [14]. MMP-9 was additionally included for its gelatinolytic activity against denatured collagen fragments, as well as its broader proteolytic action on non-collagenous ECM components including aggrecan, and collagens of types IV, V, VII, and X, as well as elastin [15]. Complementing these collagenolytic and gelatinolytic activities, ADAMTS-5 was incorporated as the dominant aggrecanase in cartilage, recognized as the principal protease responsible for aggrecan cleavage across multiple functional domains of the core protein [16]. Together, the combined proteolytic activity of these three enzymes recapitulated the major biochemical catabolic pathways active in OA and produced mechanically significant ECM degradation across both the collagenous and proteoglycan compartments of the tissue.

Overexpressed collagenase and gelatinase prevailing in cartilage lesions degrades the cartilage's structural integrity, leading to progressive damage. Under physiological conditions, regulated collagenase activity indirectly contributes to normal matrix turnover and remodeling, whereas activity due to upregulated collagenase leads to ECM degeneration [17,18]. These enzymes are transcriptionally regulated in response to joint inflammation, collectively amplifying ECM degradation within and adjacent to the damaged area [19–21]. Epidemiological and quantitative studies further confirm that osteoarthritic joints exhibit a significantly greater likelihood of developing focal cartilage lesions and of existing lesions progressing in size and severity [22,23]. While prior studies have employed either enzymatic degradation or mechanical defect models in isolation, the present work, to the best of our knowledge, is the first to systematically combine and sequence both insult modalities—enzymatic degradation and full-thickness ICRS Grade III focal defect—across five distinct experimental groups, and to comprehensively characterize their isolated and combined effects using multiple biomechanical loading modalities, including ramp compression, multi-step stress-relaxation, and dynamic cyclic loading by histomorphometric and compositional analysis.

Therefore, this study was designed to investigate the mechanical consequence of focal cartilage damage and proteolytic enzymatic degradation under physiologically relevant loading conditions, by systematically degrading bovine cartilage explants *in vitro* using a three-enzyme cocktail of MMP-13 (collagenase), MMP-9 (gelatinase), and ADAMTS-5 (aggrecanase), in isolation and in combination with an ICRS Grade III equivalent full-thickness focal defect. Five experimental groups were established to enable systematic comparison: intact healthy cartilage (Control), focal defect alone (Def), enzymatic degradation alone (Enz), enzymatic degradation followed by focal defect (Enz+Def), and focal defect followed by enzymatic degradation (Def+Enz). Each group was subjected to different testing modes comprising ramp compression, multi-step stress-relaxation, and dynamic sinusoidal loading, complemented by semi-quantitative histological analysis and Fourier transform infrared (FTIR) spectroscopy to assess collagen and PG content and their depth-wise zonal distributions across healthy and compromised ECM. However, this model does not replicate full complexity of OA, which involves additional cellular, biological, and biomechanical phenomena beyond the scope of any three-enzyme *in vitro* system; rather, the model is

designed to isolate and quantify the mechanical consequences of proteolytic ECM degradation and structural focal damage, independently and in sequence. Collectively, these findings are expected to deepen the mechanistic understanding of cartilage pathomechanics and provide a quantitative foundation for developing more targeted intervention strategies aimed at delaying OA initiation and progression.

2. Materials and methods

2.1. Sample preparation

Cylindrical osteochondral explants (n = 60) with a diameter of 9 mm were harvested from the stifle joints of six healthy adult bovines (18 - 24 months) under aseptic condition. To control anatomical site and inter-animal variability, explants were harvested solely from the weight-bearing surfaces of the femoral and tibial condyles, yielding six explants per condylar site per group with two samples collected from each stifle joint. The cartilage thickness was measured using ImageJ software from high resolution image of the sample. The average thickness of the cartilage was 1.86 ± 0.35 mm. Only samples without any visible surface damage were considered in this study. The samples were stored frozen at $-20\,^{o}$C in moist gauze soaked with phosphate buffered saline (PBS). Samples were thawed once for 45 min prior to testing.

2.2. Testing groups

Each experimental group contained 12 cartilage explants (6 per condylar site; 2 per bovine joint). The experimental group details, including treatment conditions, are summarized in Table 1.

2.3. Focal cartilage defect

A 1 mm diameter biopsy punch was used to create a central, full-thickness cylindrical defect (hole) through the articular cartilage layer to subchondral bone in all Def, Def+Enz and Enz+Def groups. The induced structural damage was designed to replicate a Grade 3 focal cartilage defect as defined by the ICRS classification [11,12]. To ensure clinical relevance, the critical *in vivo* lesion area—defined as the threshold above which focal cartilage lesions are unlikely to heal spontaneously and typically require surgical intervention—was scaled proportionally from the full joint surface (2 cm^2, representing approximately 1.23% of the 163 cm^2 total articular cartilage surface) to the explant geometry. Accordingly, a 1 mm diameter defect ($\approx$0.00785 cm^2) was introduced into the 9 mm diameter disk ($\approx$0.636 cm^2), representing approximately 1.23% of the disk surface area and maintaining the clinically derived lesion-to-surface ratio [4,24,25].

2.4. Enzymatic treatment of cartilage

The cartilage plugs were placed on sterile agar plates and gently embedded in a 2.5% solidified and autoclaved agarose gel to keep them stable during enzyme incubation, exposing only the top surface for enzyme diffusion. Samples from Enz, Enz +Def and Def+Enz groups were enzymatically treated with a mixture of MMP-9, MMP-13 and ADAMTS-5 and incubated at 37 °C for 44 h, being gently agitated every 10–12 h. Control and Def groups were also incubated under identical conditions in phosphate-buffered saline (PBS) without enzyme supplementation, ensuring observed differences between groups are attributable solely to the applied treatments. To induce proteolytic degradation of the cartilage ECM in a pathophysiologically relevant manner, enzyme concentrations similar to our groups' prior studies [26,27] were selected from the concentration range (Table 2) found in the synovial fluid of arthritic patients [28–32]. The concentrations were drawn from the range reported in OA synovial fluid to ensure pathophysiological relevance, without the supraphysiological levels associated with acute cytokine stimulation models.

Table 1
Group classification based on the treatment applied on the cartilage.

Group Name	Condition	Treatment Description
Control	Intact healthy cartilage	Healthy cartilage without any visible defect or intervention.
Defect (Def)	Focal defect alone	Cartilage with a 1 mm dia. through thickness hole (ICRS grade III defect) at the center, up to subchondral bone.
Enzyme (Enz)	Enzymatic degradation alone	Cartilage treated with MMPs-13 and –9 and ADAMTS-5 to induce enzyme mediated degradation.
Enzyme+Defect (Enz+Def)	Enzymatic degradation followed by focal defect	Localized defect of 1 mm dia. through thickness hole was induced in enzymatically degenerated cartilage.
Defect+Enzyme (Def+Enz)	Focal defect followed by enzymatic degradation	Localized defect of 1 mm dia. through thickness hole was induced in cartilage prior to enzymatic treatment.

Table 2
Concentration of MMPs-9 and 13, and ADAMTS-5, considered in this study to degrade articular cartilage *in vitro*.

Enzyme	Enzyme Concentration (ng/mL)
MMP-9	30 [28]
MMP-13	15 [29,30]
ADAMTS-5	15 [31,32]

2.5. Mechanical testing

Unconfined compressions tests were conducted on the samples using Mach-1 micromechanical testing system (Biomomentum Inc. Longueuil, QC, Canada) under three distinct loading modes (Figure 1) to characterize the mechanical properties of each experimental group. A 12 mm diameter metal non-porous platen was used consistently across all mechanical tests. Each sample was attached with its subchondral surface to a custom sample holder filled with PBS using an acrylate-based adhesive, ensuring stable specimen positioning throughout testing. To simulate the mechanical environment of prolonged standing (Figure 1a), a multi-step stress-relaxation protocol was applied, with a 5% tare prestress followed by incremental compressive steps ($3\%\,strain \times 5$, $0.1\%\,strain\,rate$) and a 180-seconds relaxation period at strain level. The equilibrium modulus was calculated from the slope of the line connecting the second to the final equilibrium stress points, thereby excluding the initial loading step to avoid pre-conditioning transients. It is acknowledged that full stress equilibrium was not achieved within the 180-second hold duration; the reported value therefore represents a pseudo-equilibrium modulus, consistent with standard practice in cartilage biomechanics [26,33,34]. Following each test, specimens were returned to the incubated environment and allowed a minimum recovery period of two hours to restore its shape and mechanical integrity prior to subsequent testing [13].

The second loading configuration was conducted in two sequential phases. In the first phase, each specimen was subjected to unconfined ramp compression to 20% total compressive strain at a strain rate of 0.1%/s, followed by a 5-minute hold at 20% strain to allow partial stress relaxation and fluid pressure equilibration, which served as mechanical prestress conditioning prior to dynamic loading. The compressive modulus was determined from the slope of the stress–strain curve in the 15–20% strain range of the unconfined ramp compression response, corresponding to the high-strain near-linear regime of

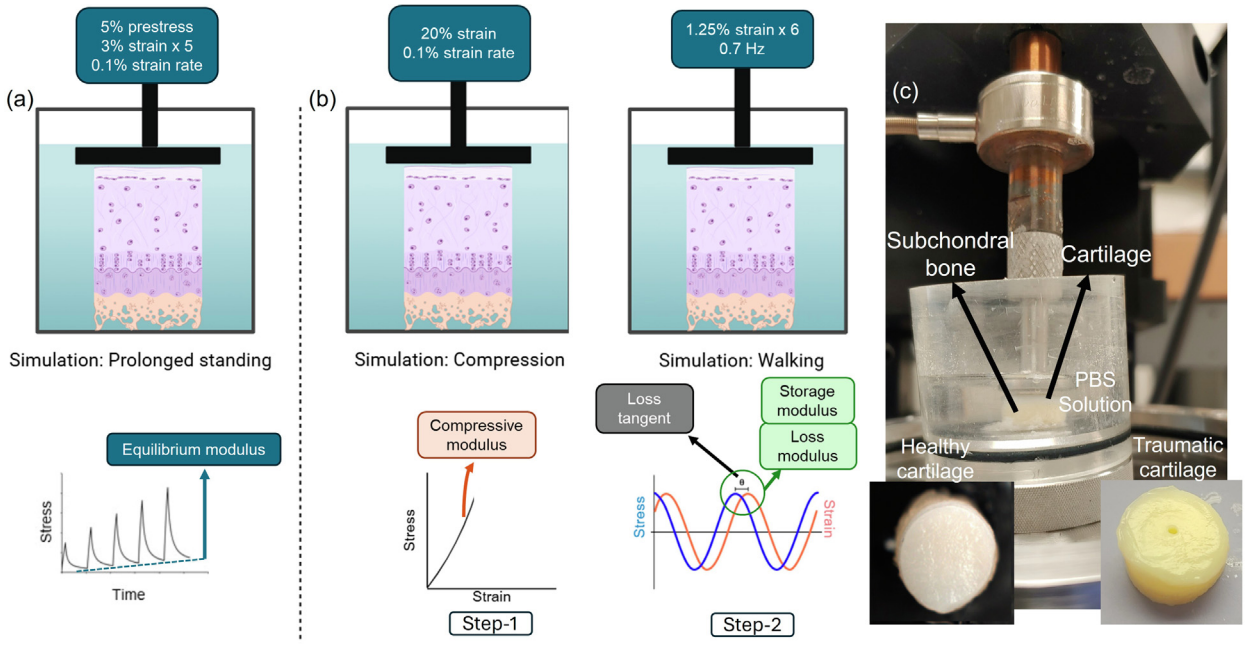

Figure 1. Systematic biomechanical testing protocol for cartilage explants. (a) Stress-relaxation test comprising a five-step incremental compression sequence at 3% strain per step, used to determine the equilibrium modulus. (b) Unconfined ramp compression test to measure compressive modulus, in which the indenter applies a ramp displacement 20% total strain at a strain rate of 0.1% [35]. Dynamic sinusoidal loading protocol applied following stress-relaxation and ramp compression, used to determine the dynamic modulus and phase difference under loading conditions representative of walking [36,37]. (c) Complete experimental setup in the Mach-1 testing system, showing the cartilage explant submerged in PBS solution and positioned beneath the compression platen for mechanical loading.

the nonlinear stress–strain response, where collagen fibril engagement is complete and tissue stiffness is maximal [35,38,39]. In the second phase, a dynamic sinusoidal loading protocol ($1.25\%\, strain\, amplitude \times 6\ cycles\ at\ 0.7Hz$) was superimposed on the 20% compressive offset strain to simulate the dynamic mechanical environment of normal walking [36,37]. The preceding prestress conditioning phase substantially attenuated the initial creep transient peak sinusoidal stress; consequently, all 6 cycles were included in the analysis. The time dependent viscoelastic properties were calculated from the peak load (F^*), peak displacement (d^*), and phase shift averaged across all cycles using Eqs. (1)–(5) [40].

$$E^* = \frac{F^*}{d^*} \tag{1}$$

$$E' = E^* \cos\delta \tag{2}$$

$$E'' = E^* \sin\delta \tag{3}$$

$$\text{Loss tangent} : \tan\delta = \frac{E''}{E'} \tag{4}$$

$$\delta = \tan^{-1}(\text{Loss tangent}) \tag{5}$$

where E^*, E', and E'' are the dynamic (complex) modulus, storage modulus, and loss modulus, respectively, and the angle δ is the phase difference between the peak force and peak displacement.

2.6. Morphological assessment

Morphological and compositional analyses were performed on $n = 3$ samples per group for both histological staining and FTIR spectroscopy. These analyses were restricted to the Control and enzymatically degraded (Enz) groups, as enzymatic degradation induces distributed, zone-wise compositional changes throughout the bulk tissue that are detectable by histological staining and FTIR spectroscopy. In contrast, the 1 mm dia. single focal mechanical defect produces a localized structural disruption confined to the lesion site, a limiting assumption that was considered in this study. Previous studies showed that ECM macromolecules following mechanical injury alone remains localized near the lesion [41], with widespread depth-wise changes occurring only when injury is combined with cytokine challenge [42,43]. In this study, the principal drivers of distant-from-defect matrix degradation such as cytokine stimulation, chondrocyte-mediated MMP secretion and inflammatory upregulation were considered absent. Accordingly, bulk FTIR and histological analyses of the Def group were not expected to reveal zone-wise compositional differences from control in regions distant from the defect margin. Moreover, sectioning through a full-thickness punch defect introduces tissue discontinuity that precludes reliable zone-wise quantification. For these reasons, the Def, Enz+Def, and Def+Enz groups were excluded from morphological and compositional analyses.

To facilitate histological analysis, articular cartilage was separated from the subchondral bone following mechanical testing to avoid decalcification process. Tissue samples were fixed in 10% neutral buffered formalin (NBF) for 12 h and dehydrated through a graded ethanol series (20%, 40%, 60%, 80%, 95%, 100%) before paraffin embedding. Afterwards, 5 μm–thick slices were sectioned with a microtome (Shandon Scientific; model: Finesse ME) [26]. After deparaffinizing, the sections were stained with Alcian blue to assess PG content under a light microscope and with Picrosirius red to evaluate collagen content and fibrillar organization, examined under a polarized light microscope (PLM).

Semi-quantitative compositional analysis of collagen and PG content was performed using a LUMOS II Bruker FTIR microscope (Bruker Optics, Billerica, MA, USA). Twenty-four attenuated total reflectance (ATR) crystal sampling points were arranged along a fixed linear transect spanning the full cartilage thickness, with 8 points distributed per zone across the superficial (SZ), middle (MZ), and deep (DZ) zones [44–47]. Each sampling point was acquired with 16 co-added scans for signal averaging at a spectral resolution of 8 cm^{-1}. Collagen and PG distributions were mapped using the amide I band (1720 to 1590 cm^{-1}) and the carbohydrate-associated peaks (1140 to 985 cm^{-1}), respectively. The semi-quantitative FTIR data was compared against the qualitative histological assessment [44,45].

Infrared signature peaks corresponding to collagen and PGs have been demonstrated to exhibit linear correlations with their respective biochemical concentrations [46]. Accordingly, relative collagen content was quantified by integrating the area under the amide I absorption band (1720–1590 cm^{-1}), and PG content was estimated by integrating the area under the carbohydrate-associated band (1140–985 cm^{-1}), which corresponds to C-O-C and C-OH vibrational modes (Figure 2). Savitzky-Golay smoothing with a second-order polynomial was used for background subtraction. No additional spectral smoothing was applied, as the 16-scan signal averaging employed during acquisition provided sufficient noise reduction for reliable peak area quantification in both the Amide I and carbohydrate spectral regions. Spectral peak area integrations were performed using a custom Python script to ensure consistent and reproducible quantification across all specimens and zones.

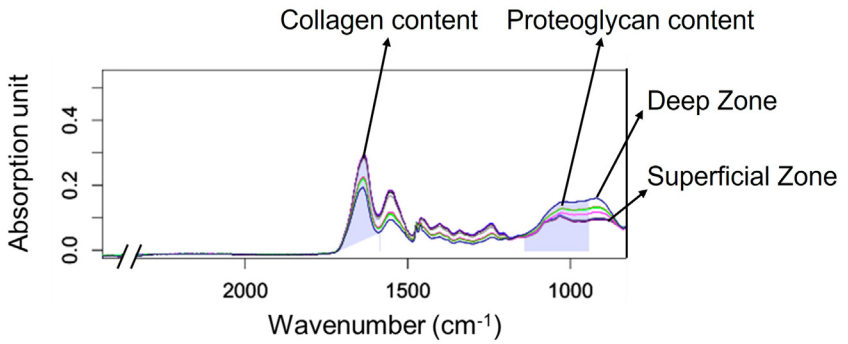

Figure 2. Representative FTIR absorption spectrum of bovine articular cartilage acquired from a single ATR sampling point within the ECM. Shaded regions indicate the baseline-corrected spectral integration windows used for semi-quantitative compositional analysis: the amide I band (1720–1590 cm^{-1}), corresponding to collagen content, and the carbohydrate band (1140–985 cm^{-1}), corresponding to PG content, shown across the SZ, MZ, and DZ of the tissue.

2.7. Statistical analysis

Statistical analyses were performed using OriginPro, Version 2025b (OriginLab Corporation, Northampton, MA) and custom Python scripts implemented in Google Colab. Normality of each outcome variable was assessed using the Shapiro–Wilk test (α = 0.05), and homogeneity of variance was evaluated using Levene's test (α = 0.05). For the equilibrium modulus, which violated the normality assumption (Shapiro–Wilk: $p > 0.05$), a Kruskal Wallis test was conducted, followed by Dunn's post hoc test with Bonferroni correction for pairwise comparisons. All remaining mechanical outcome variables satisfied the normality assumption (Shapiro-Wilk test: $p > 0.05$) but violated the homoscedasticity assumption (Levene's test: $p > 0.05$) for relatively small number of sample; these were therefore analyzed using Welch's ANOVA [48], and followed by Games-Howell post hoc test for pairwise group comparisons. A significance threshold of $p < 0.05$ was applied to all statistical tests.

3. Results

3.1. Biomechanical properties

The mechanical integrity of articular cartilage subjected to enzymatic degradation, focal defect, and their sequential combinations were assessed under three unconfined compression loading configurations as shown in Figure 1. Figure 3(a) shows

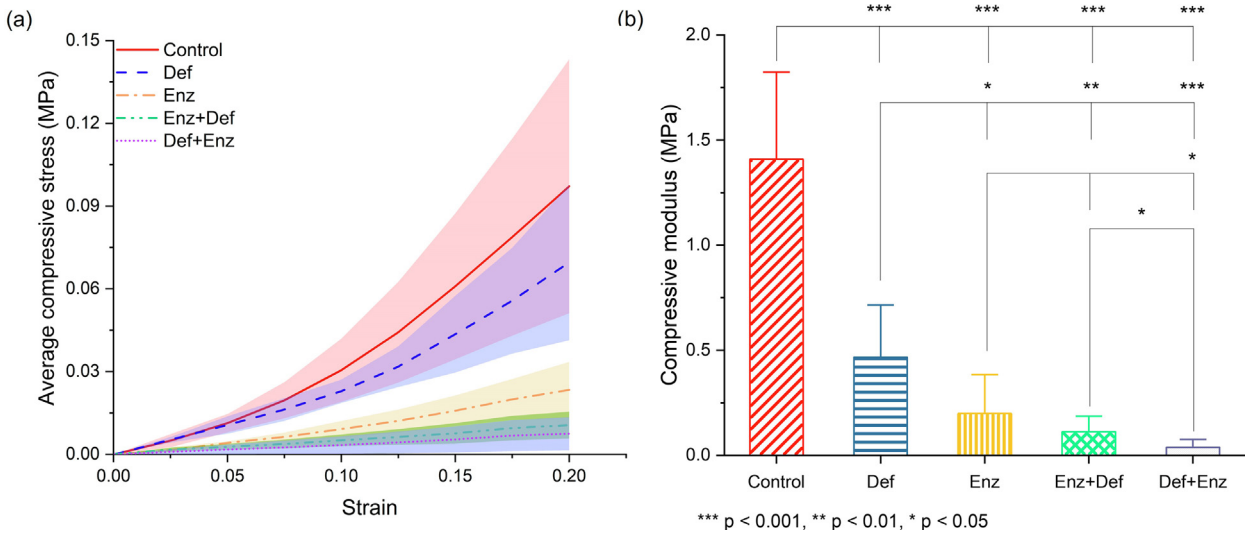

Figure 3. (a) Nonlinear compressive stress–strain behavior of intact healthy cartilage (Control), cartilage with focal defect alone (Def), enzymatically degraded cartilage (Enz), enzymatically degraded cartilage with subsequent focal defect (Enz+Def), and cartilage with focal defect followed by enzymatic degradation (Def+Enz), subjected to 20% unconfined compressive strain. Solid lines represent the group mean stress–strain response, with shaded regions denoting ± standard deviation. (b) Bar plot with error bars representing the mean ± standard deviation of compressive modulus derived from the unconfined ramp compression test for each experimental group.

the average compressive stress–strain curves for all experimental groups, with standard deviation represented by shaded regions. Both the Control and Def exhibited similar near-linear behavior up to approximately 5% strain, beyond which non-linearity increased progressively with steeper tangential slopes through 20% strain. Enzymatically degraded groups, with or without a focal defect, exhibited a pronounced reduction in stress across the full strain range. The compressive modulus was significantly reduced in all compromised groups relative to Control ($p < 0.001$) (Figure 3b). The mean compressive moduli of Control, Enz, Def, Enz+Def, and Def+Enz were1.41 ± 0.41 MPa, 0.198 ± 0.18 MPa, 0.46 ± 0.24 MPa, 0.11 ± 0.07 MPa, and 0.037 ± 0.037 MPa, respectively.

Figure 4(a) presents the stepwise stress-relaxation curves (3% strain per step, 180-second hold duration) for all 5 groups. Both peak and equilibrium stress levels varied across groups. The Control group exhibited the highest peak stress (mean: 0.04 MPa), followed by the Def group, which showed marginally lower but statistically non-significant peak stress ($p > 0.05$). The enzymatically degraded (Enz) group exhibited significantly lower peak stress (<0.02 MPa), followed by Enz+Def, with Def+Enz demonstrating the lowest peak and pseudo-equilibrium stress levels across all loading steps. Compared to the Control, the equilibrium modulus was significantly reduced in all enzymatically treated groups ($p < 0.001$), regardless of the presence of a focal defect (Figure 4b). Conversely, no statistically significant difference was observed between the Def and Control groups ($p > 0.05$). The mean equilibrium moduli of the Def, Enz, Enz+Def, and Def+Enz groups were 0.021 ± 0.013 MPa, 0.012 ± 0.007 MPa, (0.010 ± 0.006 MPa, and 0.004 ± 0.002 MPa, respectively, compared to a Control value of 0.023 ± 0.015 MPa.

Figure 5(a) illustrates the viscoelastic behavior of each group under repetitive sinusoidal loading via normalized nominal stress. The Control and Def groups exhibited comparatively denser hysteresis loops, indicative of greater energy storage capacity, with the Def group showing a marginally larger loop area than Control. In contrast, the enzymatically degraded groups displayed markedly reduced stress amplitudes and altered loop morphology relative to both Control and Def. Notably, among the enzymatically treated groups, the hysteresis loop area was largest in Def+Enz, followed by Enz+Def and Enz, indicating progressively greater energy dissipation and reduced stiffness in that order. The dynamic modulus of Control group (7.70 ± 3.59 MPa) was significantly higher than that of all the compromised groups (Figure 5b). Statistically significant differences were observed between Control and Enz+Def group (1.53 ± 1.00 MPa; $p < 0.001$), and between Control and Def +Enz group (0.92 ± 0.77 MPa; $p < 0.01$). The mean dynamic modulus of Def and Enz groups were 4.54 ± 2.58 MPa and 1.99 ± 1.34 MPa, respectively. Pairwise comparisons revealed statistically significant differences between all group pairs except Enz and Enz+Def ($p > 0.05$). The phase difference of the Control group ($27.72^\circ \pm 8.04^\circ$) was significantly lower than that of all other groups except Def ($33.60^\circ \pm 12.90^\circ$; $p > 0.05$)(Figure 5c), consistent with the more elastic mechanical behavior of intact cartilage. All remaining group pairs showed statistically significant differences ($p < 0.01$) in phase angle, with the exception of the Enz ($61.17^\circ \pm 7.04^\circ$), Enz+Def ($65.78^\circ \pm 5.64^\circ$), and Def+Enz ($66.66^\circ \pm 7.75^\circ$) comparisons ($p > 0.05$), indicating that enzymatic degradation, regardless of the presence or sequence of focal defect, produced a comparable shift toward more viscous mechanical behavior.

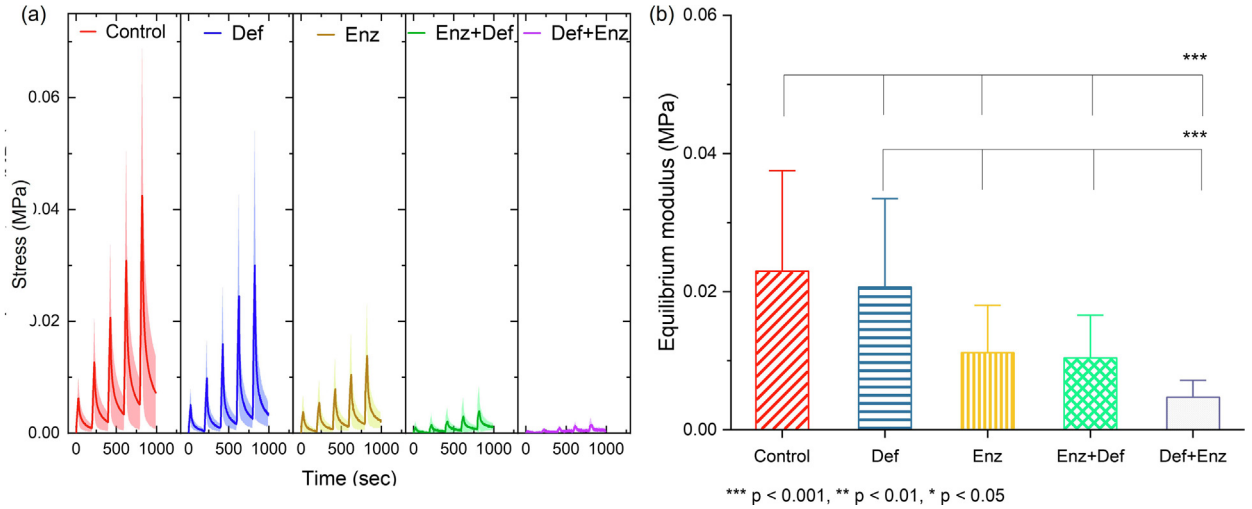

Figure 4. (a) Stress-relaxation behavior of intact healthy cartilage (Control), cartilage with focal defect alone (Def), enzymatically degraded cartilage (Enz), enzymatically degraded cartilage with subsequent focal defect (Enz+Def), and cartilage with focal defect followed by enzymatic degradation (Def+Enz) comprising a five-step incremental compression sequence at 3% strain per step. Solid lines represent the group mean stress–strain response, with shaded regions denoting ± standard deviation. (b) Bar plots with error bars representing the mean ± standard deviation of equilibrium modulus derived from the five-step stress relaxation test for each experimental group.

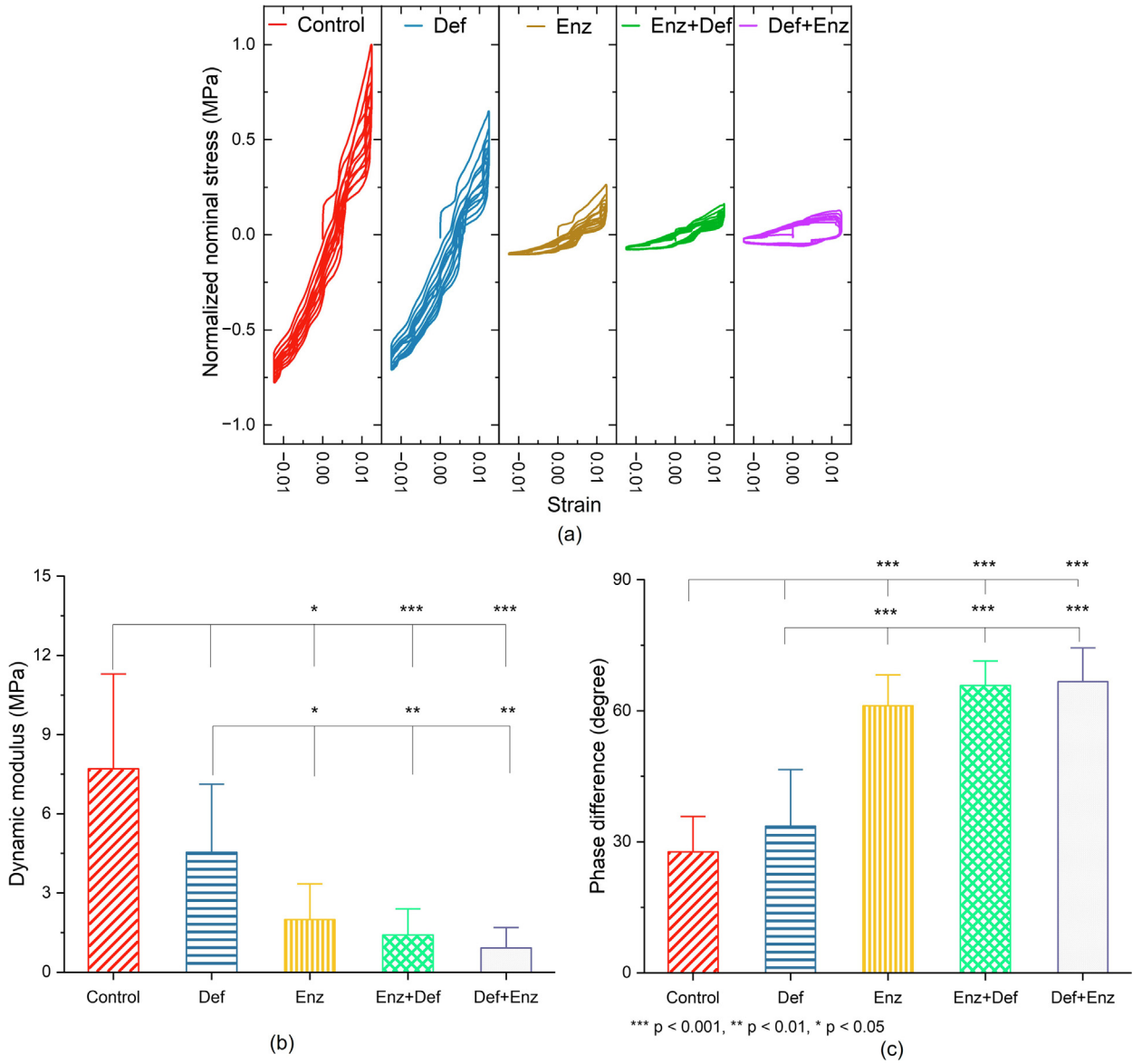

Figure 5. (a) Normalized nominal stress–time hysteresis loops under sinusoidal loading (1.25% strain amplitude × 6 cycles at 0.7 Hz, superimposed on 20% compressive offset strain) for intact healthy cartilage (Control), cartilage with focal defect alone (Def), enzymatically degraded cartilage (Enz), enzymatically degraded cartilage with subsequent focal defect (Enz+Def), and cartilage with focal defect followed by enzymatic degradation (Def+Enz). Bar plots with error bars representing the mean ± standard deviation of (b) dynamic modulus and (c) phase difference for all experimental groups under dynamic sinusoidal loading simulating normal walking.

3.2. Morphological and compositional evaluation

3.2.1. Assessment of proteoglycans

Alcian blue staining enabled zone-specific visualization of PG distribution under light-microscope (Figure 6a, and b). In both healthy and enzymatically degraded cartilage, staining intensity was highest in the DZ and decreased progressively through the MZ and SZ, consistent with the known depth-dependent PG distribution in native cartilage. However, staining intensity was uniformly reduced across all three zones in enzymatically degraded tissue relative to healthy controls, indicating widespread PG depletion.

FTIR carbohydrate band mapping (1140–985 cm^{-1}) across 24 ATR sampling points corroborated these histological observations (Figure 6c and d). Healthy cartilage exhibited highest carbohydrate band absorption in DZ, which decreased through MZ to SZ. In enzymatically degraded cartilage, absorption was uniformly reduced across all zones (Figure 6d), further confirming zone-wise PG depletion. The zone-wise bar plot (Figure 6e) revealed significantly higher PG content in the DZ of

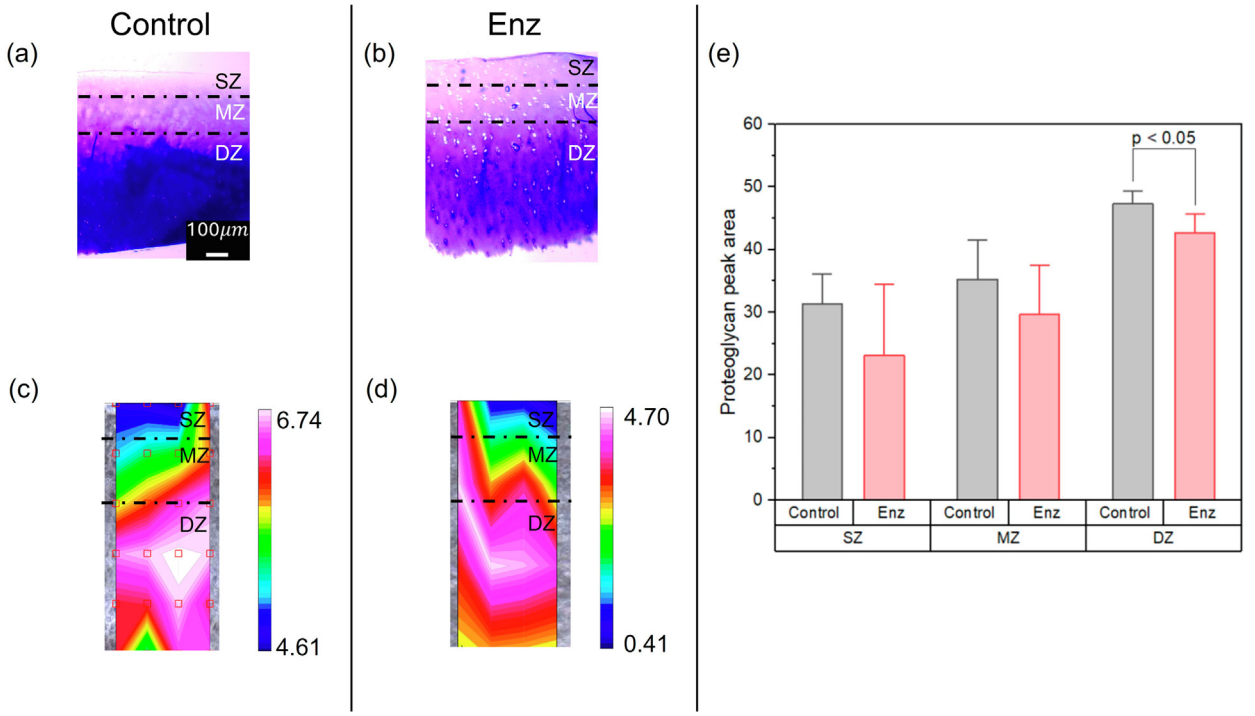

Figure 6. PG content and zone-wise distribution in healthy and enzymatically degraded of articular cartilage observed in Alcian blue stained micrographs and FTIR images. Alcian blue-stained micrographs acquired under light microscope illustrate zone-wise variations in PG content and its distribution in (a) healthy (Control) and (b) enzymatically degraded (Enz) cartilage. FTIR peak integration maps of the carbohydrate band depict the relative zone-wise PG distribution and content of PGs in (c) healthy (Control) and (d) enzymatically degraded (Enz) cartilage. Black dotted lines demarcate the SZ, MZ, and DZ boundaries in all images. (e) Bar plot comparing zone-wise PG content between healthy and enzymatically degraded cartilage groups. Error bars represent the 95% confidence interval (CI). (For interpretation of the references to colour in this figure legend, the reader is referred to the web version of this article.)

healthy cartilage relative to the degraded group ($p < 0.05$). PG content in SZ and MZ was also reduced in degraded cartilages, although to a lesser degree than in DZ.

3.2.2. Assessment of type II collagen

Polarized light micrographs of Picrosirius red-stained samples revealed zone-specific differences in collagen fibril content, organization, and birefringence between healthy and enzymatically degraded cartilage (Figure 7a, and b). In healthy cartilage, the SZ exhibited densely packed, well-organized collagen fibrils appearing as bright yellow or yellowish-orange birefringence, consistent with a thick, highly oriented fibrillar architecture. The DZ contained comparatively thinner fibrils appearing as green birefringence, reflecting the more randomly oriented DZ collagen network [49–51]. In enzymatically degraded cartilage compared to Control, birefringence intensity was reduced across all zones, indicating disruption of fibrillar organization and loss of collagen content (Figure 7b).

Semi-quantitative FTIR mapping of the Amide I band (1720–1590 cm^{-1}) confirmed the histological observations in healthy (Figure 7c) and degraded (Figure 7d) cartilage. In healthy cartilage, Amide I absorption was highest in DZ and decreased progressively through the MZ to SZ, consistent with the depth-dependent collagen content gradient in native tissue. Enzymatically degraded cartilage exhibited uniformly reduced Amide I absorption across all zones, indicating zone-wise collagen loss. The zone-wise bar plot (Figure 7e) confirms that collagen content increased incrementally from SZ to DZ in healthy cartilage, and that significantly higher collagen content was present in each zone of the Control group relative to the enzymatically degraded group ($p < 0.05$).

4. Discussion

The goal of this study was to develop a comprehensive understanding of the biomechanics of mechanically damaged and enzymatically degraded, and their sequential combination in articular cartilage, which are pathological features collectively characteristic of osteoarthritic cartilage. In this *in vitro* study, a cocktail of MMPs-13 and –9 and ADAMTS-5 was used to degrade collagen and PGs, in combination with a full-thickness focal cartilage defect extending to the subchondral bone, to systematically compromise the ECM's load-bearing capacity in a manner representative of osteoarthritic cartilage. In this work, the morpho-mechanical outcomes of these insults, individually and in combination, were investigated through

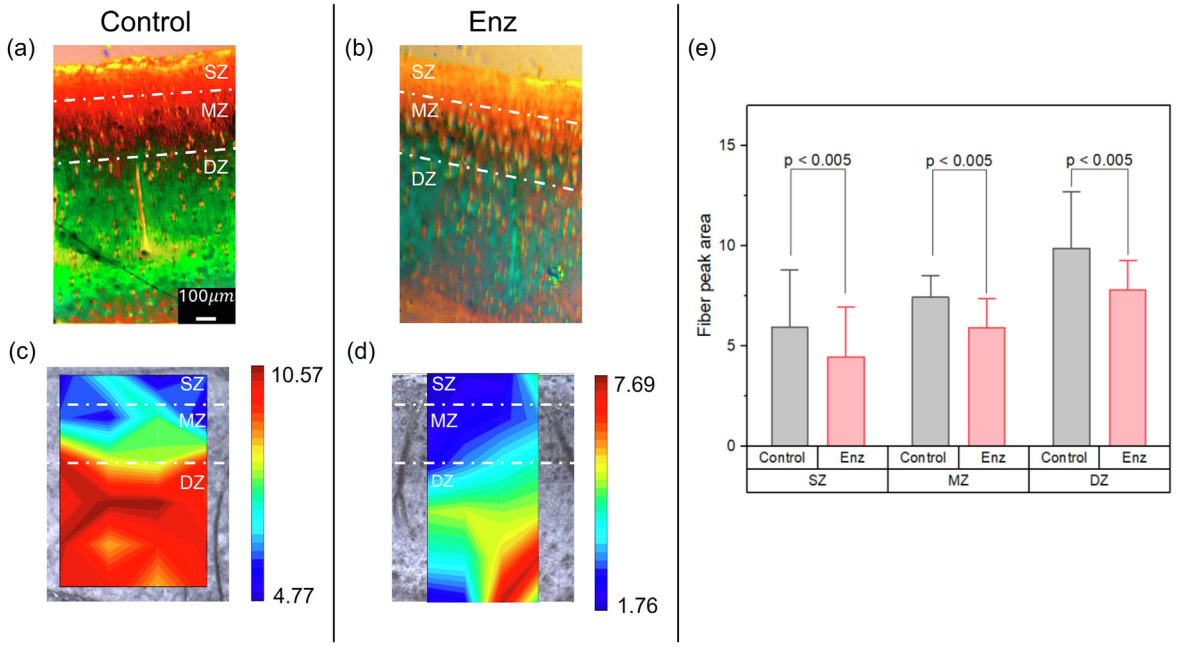

Figure 7. Zone-wise collagen content, distribution, and fibrillar organization in healthy and enzymatically degraded articular cartilage assessed by Picrosirius red staining under PLM and FTIR spectroscopy. Picrosirius red stained polarized light micrographs illustrate zone-specific content and orientation of collagen fibril in (a) healthy (Control) and (b) enzymatically degraded (Enz) cartilage. FTIR peak integration maps of Amide I band depict the relative zone-wise collagen content and distribution in (c) healthy (Control) and (d) enzymatically degraded (Enz) cartilage. White dotted lines demarcate the SZ, MZ, and DZ boundaries in all images. (e) Bar plot comparing zone-wise collagen content between healthy (Controls) and enzymatically degraded (Enz) cartilage groups. Error bars represent the 95% C.I. (For interpretation of the references to colour in this figure legend, the reader is referred to the web version of this article.)

histo-mechanical analyses. To the best of our knowledge, this is the first study to systematically combine and sequence enzymatic degradation and a full-thickness ICRS Grade III focal defect across five experimental groups, while characterizing their mechanical properties under multiple loading configurations and providing depth-resolved compositional validation through FTIR spectroscopy and histomorphometry—offering mechanistic resolution that neither approach alone has previously achieved.

MMP-13 (collagenase), the principal collagenolytic enzyme in OA, cleaves type II collagen with high substrate specificity and catalytic efficiency [52], at a significantly accelerated rate compared to other collagenases [53]. MMP-9 (gelatinase) was included for its complementary activity in degrading denatured collagen fragments and non-fibrillar matrix constituents, synergizing with MMP-13, to recapitulate the advanced osteoarthritic catabolic condition. In addition to its primary collagenolytic activity, MMP-13 contributes more broadly to ECM breakdown by degrading aggrecan and other non-collagenous matrix components [54,55]. This enzymatic action is evident in the degraded cartilage histology (Figure 6), which shows substantial collagen depletion in SZ, as well as noticeable degradation in DZ, reflecting the broad spatial range of enzyme activity across the full tissue thickness. Disruption of the collagen network impaired its ability to structurally support PGs, which in turn increased interstitial fluid exudation and reduced tissue stiffness under dynamic loading (Figure 5) [56,57]. PGs are critical modulators of cartilage mechanics, regulating permeability and resisting rapid deformation under compressive load [58,59]. ADAMTS-5 (aggrecanase) specifically penetrates the aggrecan core protein, producing rapid and extensive PG depletion [60,61]. The combined proteolytic activity of these enzymes was reflected in the 2.09-fold reduction in equilibrium modulus between degraded and healthy groups under stress-relaxation conditions, closely matching the decline in compressive modulus—attributable primarily due to PG depletion, with a contributory role of collagen degradation [62,63]. It should be noted that the enzyme concentrations employed here were not intended to represent normal physiological protease activity in healthy cartilage, where MMPs and ADAMTS activity is tightly regulated by endogenous inhibitors (TIMPs, α2-macroglobulin) and remains at largely undetectable levels in synovial fluid. Rather, the selected concentrations model the pathological catabolic microenvironment of moderate-to-advanced OA or post-injury inflammatory states, wherein inhibitor balance is disrupted, and net ECM catabolism dominates. Accordingly, the enzyme-treated groups (Enz, Enz+Def, Def+Enz) represent an OA-compromised joint microenvironment, while the Def group represents an acute mechanical injury in an otherwise biochemically intact joint, analogous to an isolated traumatic cartilage lesion without concurrent enzymatic upregulation.

Focal structural damage disrupts the continuity of the type II collagen fibrillar network within the ECM, producing stress amplification at the defect margins [64] and significant alteration of the elastic response under physiological compressive loading [65,66]. Focal defects also perturb the local PG distribution, facilitating interstitial fluid and solute egress, and consequent PG loss, preceding any gross changes in collagen network [41]. Prior studies demonstrated that 1 mm cracks in cartilage can reduce the compressive strength by approximately half, attributable to loosening of the fibrillar weave [67,68]. The present findings are consistent with this observation The stress–strain curve of the Def group closely resembled that of the Control up to approximately 5% compressive strain, beyond which the Def group stress progressively diverged with continued loading (Figure 3a). Under stress-relaxation conditions, the collagen network primarily supports peak compressive stress, while entrapped PGs contribute to equilibrium stiffening during the relaxation phase [69,70]. Disruption of the ECM architecture by the focal defect increases collagen fibril mobility, providing less structural constraint, and thereby reducing the peak stress of mechanically damaged cartilage (Figure 4a) [70]. The stress–strain (Figure 3a) and normalized stress–time (Figure 4a) responses indicate that bulk mechanical softening is primarily driven by the degradative proteases, while an isolated focal defect produces only minimal ECM softening. Focal cartilage defect alone contributed to 66.9% ($p < 0.001$, 95% CI : [42.1%, 81.1%]) lower compressive modulus and 10.1% ($p > 0.05$, 95% CI : [−63.1%, 14.4%]) lower equilibrium modulus compared with Control group. The structural damage associated with the defect also impaired viscoelastic energy storage and dissipation capacity. Swelling of the PG-rich matrix adjacent to the defect site contributed to reduced energy dissipation during dynamic loading [68,71]. The dynamic modulus of Def group was 40.1% ($p < 0.05$, 95% CI : [6.1%, 62.7%]) lower than Control; however, the phase difference of the Def group was 21.2% ($p > 0.05$, 95% CI : [−1.5%, 49.3%]) higher than Control, reflecting increased energy dissipation attributable to structural disruption of the collagen fibrillar network at the defect site (Figure 5).

This study evidently shows that enzymatic degradation is considerably more detrimental to the structural integrity of cartilage than an isolated focal mechanical defect. The combined effects of focal defect and enzymatic degradation (Enz +Def and Def+Enz groups) produced lower mechanical properties than either insult in isolation. Cartilage mechanics were most severely compromised in the Enz+Def and Def+Enz groups (Figure 3a and a), where the structural integrity of ECM was disrupted by both modalities simultaneously. The equilibrium modulus of the Enz+Def group was approximately 54.8% ($p < 0.05$, 95% CI : [7.0%, 65.8%]) lower than the Control, whereas the compressive modulus was significantly reduced by 92.0% ($p < 0.05$, 95% CI : [21.6%, 102.4%]). However, near-equivalence of equilibrium modulus and the minimal differences in compressive and dynamic moduli between Enz and Enz+Def clearly demonstrate that introduction of a mechanical defect following prior enzymatic degradation produces comparatively limited additional mechanical deterioration. In contrast, a focal defect introduced prior to enzymatic exposure created a more permissive environment for matrix dissolution, producing the lowest static and dynamic moduli across all experimental groups. The pre-existing focal defect in the Def+Enz group facilitated enhanced enzyme diffusion into the ECM through the structural discontinuity, thereby amplifying the extent of proteolytic degradation. Consequently, the equilibrium modulus of Def+Enz group was approximately 79.7% ($p < 0.001$, 95% CI : [58.1%, 90.1%]) lower than the Control, and the compressive modulus was significantly reduced by 97.7% ($p < 0.001$, 95% CI : [95.1%, 98.9%]). The breakdown of collagen and PGs by degradative enzyme activity thus produced pronounced ECM degradation, significantly reducing the compressive modulus in all enzyme-mediated groups (Figure 3b). Interestingly, while statistically significant differences in static elastic properties were observed between the Enz+Def and Def+Enz groups, their viscoelastic properties exhibited comparatively smaller differences (Figure 5). The enlarged hysteresis loop area (Figure 5a) reflects greater energy dissipation and reduced stiffness—evidenced by lower storage and dynamic modulus—consequent to PG depletion, which was most pronounced in the enzyme-mediated group (Figure 6). The hysteresis loop area increased when a focal defect was introduced into enzymatically degraded cartilage (Enz+Def) and was largest when the defect preceded enzymatic treatment (Def+Enz). The differences in dynamic modulus and phase difference between the Def+Enz and Enz+Def groups were 21.1% ($p > 0.05$, 95% CI : [−66.3%, 84.7%]) and 1.8% ($p > 0.05$, 95% CI : [−48.5%, 101.6%]), respectively.

Despite the mechanistically informative findings, several limitations of this study should be acknowledged. First, the outcomes were based on a moderately sized focal defect scaled to maintain a clinically relevant defect-to-surface area ratio; cartilage specimens with larger defects or multiple fissures may provide additional mechanistic insight but risk catastrophic tissue failure under *in vitro* mechanical loading, precluding reliable biomechanical assessment. Second, morphological and compositional analyses were restricted to the Control and Enz groups. The current study did not directly assess compositional changes in the Def group based on the limiting assumption that compositional disruption due to the focal defect would remain localized to the lesion site. Additionally, in the absence of cytokine stimulation and chondrocyte-mediated catabolic signaling, widespread zone-wise compositional changes distant from the defect site were not expected over the 44-hour incubation period [26,27,42,43]. However, the possibility of minor peri-defect compositional alterations beyond the immediate lesion margin cannot be formally excluded. This represents a limitation of the study design. Future work employing spatially resolved techniques such as Raman spectroscopy or nanoindentation mapping adjacent to the defect margin would provide more targeted peri-defect compositional characterization. Third, the enzyme cocktail (MMP-9, MMP-13, ADAMTS-5) recapitulates key OA-related catabolic pathways but does not fully replicate the *in vivo* microenvironment, which additionally involves cytokine signaling, chondrocyte-mediated anabolic-catabolic responses, and temporal inhibitor regulation. Furthermore, this model does not fully replicate the osteoarthritic disease process. OA involves additional phenomena including cytokine-mediated chondrocyte dysfunction, synovial inflammation, subchondral bone remodeling, and progressive *in vivo* loading history that are not captured by a three-enzyme *in vitro* system. The enzyme cocktail was selected to

target the primary protease classes responsible for ECM breakdown (collagenase, gelatinase, aggrecanase) at pathophysiologically relevant concentrations, rather than to simulate the full OA microenvironment. Fourth, full thermodynamic equilibrium was not reached within 180-second hold periods; the reported equilibrium modulus therefore represents a pseudo-equilibrium value consistent with established practice in cartilage biomechanics. Fifth, flow-dependent poroelastic parameters, specifically hydraulic permeability, were not directly quantified in this study. The multi-step stress-relaxation and dynamic loading protocols capture the integrated poroviscoelastic response of the tissue; future work employing confined compression biphasic analysis or fibril-reinforced poroelastic modelling would provide further mechanistic resolution between flow-dependent and flow-independent contributions to the observed mechanical degradation. Next, the sequential Def+Enz and Enz+Def groups nonetheless serve as mechanistic surrogates for two clinically relevant temporal scenarios: acute cartilage injury in a pre-existing enzyme-rich inflammatory joint (Def+Enz), and progressive enzymatic upregulation following chronic mechanical insult (Enz+Def), with the finding that Def+Enz produces the most severe mechanical deterioration carrying direct clinical implications for early intervention in patients with focal cartilage lesions concurrent with underlying inflammatory or metabolic joint disease. This temporal dynamics of OA progression, wherein mechanical injury gradually upregulates enzymatic activity over months, is not fully captured by the acute sequential *in vitro* approach; this is a recognized limitation of all *in vitro* degradation models. Next, Picrosirius red staining and the FTIR amide I band assess total collagen rather than type II collagen specifically; type II collagen-specific immunohistochemistry would provide greater compositional resolution. Finally, adult bovine cartilage introduces biological variability associated with age, loading history, and inter-animal heterogeneity, and may not fully represent the mechanical behavior or compositional organization of human cartilage under clinical conditions.

In conclusion, enzymatic degradation plays a dominant role in compromising cartilage mechanical integrity, with enzymatically degraded cartilage exhibiting substantially greater deterioration in compressive, equilibrium, and dynamic mechanical properties relative to cartilage with an isolated focal defect. While the sequential combination of focal defect and enzymatic degradation produced the lowest overall mechanical response, the order of insult introduction had a significant and mechanistically distinct influence on the magnitude of mechanical deterioration across all loading modalities. Specifically, a moderate focal cartilage defect introduced prior to enzymatic exposure significantly amplified the loss of morpho-mechanical properties relative to enzymatic degradation alone, independent of the testing mode—attributable to enhanced enzyme diffusion through the structural discontinuity of the pre-existing defect. From a clinical perspective, these findings underscore the importance of early surgical or pharmacological intervention in patients presenting with focal cartilage lesions, particularly those with underlying metabolic or inflammatory conditions associated with elevated catabolic enzyme activity, in whom the synergistic interaction between structural damage and enzymatic upregulation may substantially accelerate cartilage deterioration.

CRediT authorship contribution statement

Asif Istiak: Writing – review & editing, Writing – original draft, Visualization, Validation, Methodology, Investigation, Formal analysis, Data curation, Conceptualization. **Ahmed Suparno Bahar Moni:** Supervision, Conceptualization. **Tanvir R. Faisal:** Writing – review & editing, Validation, Supervision, Funding acquisition, Conceptualization, Software.

Declaration of competing interest

The authors declare that they have no known competing financial interests or personal relationships that could have appeared to influence the work reported in this paper.

Acknowledgements

We acknowledge the assistance of Austin Lawrence and Joseph Boesel from the Department of Orthopedics and Medical Education, College of Medicine and Life Sciences, University of Toledo for the help in extracting the cartilage explants and their enzymatic degradation.

Role of the funding sources

The work is supported by Louisiana Board of Regents Research Competitive Subprogram (RCS) funds (Grant No# LEQSF (2025-28)-RD-A-17).

References

[1] Ouyang Z, Dong L, Yao F, Wang K, Chen Y, Li S, et al. Cartilage-related collagens in osteoarthritis and rheumatoid arthritis: from pathogenesis to therapeutics. Int J Mol Sci 2023;24(12):9841.
[2] Kiani C, Chen L, Wu YJ, Yee AJ, Yang BB. Structure and function of aggrecan. Cell Res 2002;12(1):19–32.
[3] Borrelli Jr J, Olson SA, Godbout C, Schemitsch EH, Stannard JP, Giannoudis PV. Understanding articular cartilage injury and potential treatments. J Orthop Trauma 2019;33:S6–S12.

[4] Jarecki J, Waśko MK, Widuchowski W, Tomczyk-Warunek A, Wójciak M, Sowa I, et al. Knee cartilage lesion management—current trends in clinical practice. J Clin Med 2023;12(20):6434.
[5] Articular R-M. cartilage defects of the knee: diagnosis and treatment. Springer Science & Business Media; 2012.
[6] Hjelle K, Solheim E, Strand T, Muri R, Brittberg M. Articular cartilage defects in 1000 knee arthroscopies. Arthros: J Arthros Rel Surg 2002;18(7):730–4.
[7] Curl WW, Krome J, Gordon ES, Rushing J, Smith BP, Poehling GG. Cartilage injuries: a review of 31,516 knee arthroscopies. Arthros: J Arthros Rel Surg 1997;13(4):456–60.
[8] Jamil T, Ansari U, Ali MN, Mir M. A review on biomechanical and treatment aspects associated with anterior cruciate ligament. Irbm 2017;38(1):13–25.
[9] Merkely G, Ackermann J, Lattermann C. Articular cartilage defects: incidence, diagnosis, and natural history. Operat Tech Sports Med 2018;26(3):156–61. doi: https://doi.org/10.1053/j.otsm.2018.06.008.
[10] Steinmetz RG, Guth JJ, Matava MJ, Smith MV, Brophy RH. Global variation in studies of articular cartilage procedures of the knee: a systematic review. Cartilage 2022;13(2):19476035221098169. doi: https://doi.org/10.1177/19476035221098169.
[11] Browne JE, Branch TP. Surgical alternatives for treatment of articular cartilage lesions. JAAOS-J Am Acad Orthop Surg 2000;8(3):180–9.
[12] Van den Borne M, Raijmakers N, Vanlauwe J, Victor J, De Jong S, Bellemans J, et al. International Cartilage Repair Society (ICRS) and oswestry macroscopic cartilage evaluation scores validated for use in autologous chondrocyte implantation (ACI) and microfracture. Osteoarthr Cartil 2007;15(12):1397–402.
[13] Mixon A, Savage A, Bahar-Moni AS, Adouni M, Faisal T. An in vitro investigation to understand the synergistic role of MMPs-1 and 9 on articular cartilage biomechanical properties. Sci Rep 2021;11(1):14409. doi: https://doi.org/10.1038/s41598-021-93744-1.
[14] Acharya C, Yik JH, Kishore A, Van Dinh V, Di Cesare PE, Haudenschild DR. Cartilage oligomeric matrix protein and its binding partners in the cartilage extracellular matrix: interaction, regulation and role in chondrogenesis. Matrix Biol 2014;37:102–11.
[15] Mukherjee A, Das B. The role of inflammatory mediators and matrix metalloproteinases (MMPs) in the progression of osteoarthritis. Biomat Biosyst 2024;13:100090. doi: https://doi.org/10.1016/j.bbiosy.2024.100090.
[16] Jiang L, Lin J, Zhao S, Wu J, Jin Y, Yu L, et al. ADAMTS5 in osteoarthritis: biological functions, regulatory network, and potential targeting therapies. Front Mol Biosci 2021;8. doi: https://doi.org/10.3389/fmolb.2021.703110.
[17] Kevorkian L, Young DA, Darrah C, Donell ST, Shepstone L, Porter S, et al. Expression profiling of metalloproteinases and their inhibitors in cartilage. Arth Rheum: Off J Am Coll Rheumat 2004;50(1):131–41.
[18] Li T, Peng J, Li Q, Shu Y, Zhu P, Hao L. The mechanism and role of ADAMTS protein family in osteoarthritis. Biomolecules 2022;12(7):959.
[19] Yang C-Y, Chanalaris A, Troeberg L. ADAMTS and ADAM metalloproteinases in osteoarthritis–looking beyond the 'usual suspects'. Osteoarthr Cartil 2017;25(7):1000–9.
[20] Malemud CJ. Inhibition of MMPs and ADAM/ADAMTS. Biochem Pharmacol 2019;165:33–40.
[21] Tetsunaga T, Nishida K, Furumatsu T, Naruse K, Hirohata S, Yoshida A, et al. Regulation of mechanical stress-induced MMP-13 and ADAMTS-5 expression by RUNX-2 transcriptional factor in SW1353 chondrocyte-like cells. Osteoarthr Cartil 2011;19(2):222–32.
[22] Bae WC, Payanal MM, Chen AC, Hsieh-Bonassera ND, Ballard BL, Lotz MK, et al. Topographic patterns of cartilage lesions in knee osteoarthritis. Cartilage 2010;1(1):10–9.
[23] Alizai H, Virayavanich W, Joseph GB, Nardo L, Liu F, Liebl H, et al. Cartilage lesion score: comparison of a quantitative assessment score with established semiquantitative MR scoring systems. Radiology 2014;271(2):479–87.
[24] Cohen ZA, Mccarthy DM, Kwak SD, Legrand P, Fogarasi F, Ciaccio EJ, et al. Knee cartilage topography, thickness, and contact areas from MRI: in-vitro calibration and in-vivo measurements. Osteoarthr Cartil 1999;7(1):95–109.
[25] Eckstein F, Winzheimer M, Hohe J, Englmeier K-H, Reiser M. Interindividual variability and correlation among morphological parameters of knee joint cartilage plates: analysis with three-dimensional MR imaging. Osteoarthr Cartil 2001;9(2):101–11.
[26] Istiak A, Lawrence A, Boesel J, Kayes MI, Moni ASB, Faisal TR. Therapeutic potential of COMP and TIMP-3 in preserving cartilage integrity compromised by proteases: a histo-mechanical study. J Mech Behav Biomed Mater 2025:107183. doi: https://doi.org/10.1016/j.jmbbm.2025.107183.
[27] Lawrence A, Boesel J, Beier K, Ratiani L, Unrein H, Moni ASB. Enzymatic drivers of cartilage breakdown: insights from a bovine osteoarthritis explant model. Orthop Surg 2026;18(1):138–45. doi: https://doi.org/10.1111/os.70202.
[28] Stojanović S, Stamenković B, Nedovic J, Živković V, Aleksic I. AB0227 baseline synovial levels of matrix metalloproteinases-9 in early rheumatoid arthritis-the association with initial radiographic changes. Ann Rheum Dis 2020;79:1413–4.
[29] Wang X, Manner PA, Horner A, Shum L, Tuan RS, Nuckolls GH. Regulation of MMP-13 expression by RUNX2 and FGF2 in osteoarthritic cartilage. Osteoarthr Cartil 2004;12(12):963–73.
[30] Heard BJ, Martin L, Rattner JB, Frank CB, Hart DA, Krawetz R. Matrix metalloproteinase protein expression profiles cannot distinguish between normal and early osteoarthritic synovial fluid. BMC Musculoskelet Disord 2012;13:1–12.
[31] Zhang E, Yan X, Zhang M, Chang X, Bai Z, He Y, et al. Aggrecanases in the human synovial fluid at different stages of osteoarthritis. Clin Rheumatol 2013;32:797–803.
[32] Hao X, Wu X. SP1 mediated ADAMTS5 transcription promotes IL 1β induced chondrocyte injury via Wnt/β catenin pathway in osteoarthritis. Mol Med Rep 2024;30(2):149.
[33] Khajehsaeid H, Abdollahpour Z, Farahmandpour H. Effect of degradation and osteoarthritis on the viscoelastic properties of human knee articular cartilage: an experimental study and constitutive modeling. Biomechanics 2021;1(2):225–38. , https://www.mdpi.com/2673-7078/1/2/19.
[34] Brinkhof S, Froeling M, Janssen RP, Ito K, Klomp DW. Can sodium MRI be used as a method for mapping of cartilage stiffness? MAGMA 2021;34(3):327–36.
[35] Istiak A, Islam S, Adouni M, Faisal TR. Hyperelastic constitutive modeling of healthy and enzymatically mediated degraded articular cartilage. Biomech Model Mechanobiol 2025;24(2):471–87. doi: https://doi.org/10.1007/s10237-024-01919-2.
[36] Strutzenberger G, Claußen L, Schwameder H. Analysis of sloped gait: how many steps are needed to reach steady-state walking speed after gait initiation? Gait Posture 2021;83:167–73.
[37] Niehoff A, Müller M, Brüggemann L, Savage T, Zaucke F, Eckstein F, et al. Deformational behaviour of knee cartilage and changes in serum cartilage oligomeric matrix protein (COMP) after running and drop landing. Osteoarthr Cartil 2011;19(8):1003–10.
[38] Kabir W, Di Bella C, Choong PFM, O'Connell CD. Assessment of native human articular cartilage. A biomechanical protocol. Cartilage 2021;13(2_suppl):427s–37s. doi: https://doi.org/10.1177/1947603520973240.
[39] Fortin M, Soulhat J, Shirazi-Adl A, Hunziker E, Buschmann M. Unconfined compression of articular cartilage: nonlinear behavior and comparison with a fibril-reinforced biphasic model. J Biomech Eng 2000;122(2):189–95.
[40] Lawless BM, Barnes SC, Espino DM, Shepherd DE. Viscoelastic properties of a spinal posterior dynamic stabilisation device. J Mech Behav Biomed Mater 2016;59:519–26.
[41] Elahi SA, Castro-Viñuelas R, Tanska P, Korhonen R, Lories R, Famaey N, et al. Contribution of collagen degradation and proteoglycan depletion to cartilage degeneration in primary and secondary osteoarthritis: an in silico study. Osteoarthr Cartil 2023;31(6):741–52.
[42] Hamada M, Eskelinen ASA, Florea C, Mikkonen S, Nieminen P, Grodzinsky AJ, et al. Loss of collagen content is localized near cartilage lesions on the day of injurious loading and intensified on day 12. J Orthop Res 2025;43(1):70–83. doi: https://doi.org/10.1002/jor.25975.
[43] Hamada M, Eskelinen AS, Kosonen JP, Florea C, Grodzinsky AJ, Tanska P, et al. MMP release following cartilage injury leads to collagen loss in intact tissue: a computational study. PLoS Comput Biol 2026;22(1):e1013209.
[44] Kim M, Bi X, Horton Jr WE, Spencer RG, Camacho NP. Fourier transform infrared imaging spectroscopic analysis of tissue engineered cartilage: histologic and biochemical correlations. J Biomed Opt 2005;10(3):031105–6.
[45] Kim M, Foo LF, Uggen C, Lyman S, Ryaby JT, Moynihan DP, et al. Evaluation of early osteochondral defect repair in a rabbit model utilizing Fourier transform–infrared imaging spectroscopy, magnetic resonance imaging, and quantitative T2 mapping. Tissue Eng Part C Methods 2010;16(3):355–64.

[46] Camacho NP, West P, Torzilli PA, Mendelsohn R. FTIR microscopic imaging of collagen and proteoglycan in bovine cartilage. Biopol: Orig Res Biomol 2001;62(1):1–8.
[47] Mambiri LT, Guillory R, Depan D. Thermoresponsive behavior, degradation, and bioactivity of nanohydroxyapatite on graphene oxide nanoscroll-enhanced Poly(N-isopropylacrylamide)-based scaffolds. Polymers 2025;17(15):2014. , https://www.mdpi.com/2073-4360/17/15/2014.
[48] Maenohara Y, Chijimatsu R, Tachibana N, Uehara K, Xuan F, Mori D, et al. Lubricin contributes to homeostasis of articular cartilage by modulating differentiation of superficial zone cells. J Bone Miner Res 2020;36(4):792–802.
[49] Cristoforetti A, Masè M, Ravelli F. Model-based approach for the semi-automatic analysis of collagen birefringence in polarized light microscopy. Appl Sci 2023;13(5):2916.
[50] Coelho PGB, Souza MV, Conceição LG, Viloria MIV, Bedoya SAO. Evaluation of dermal collagen stained with picrosirius red and examined under polarized light microscopy. An Bras Dermatol 2018;93(3):415–8.
[51] Schmitz N, Laverty S, Kraus V, Aigner T. Basic methods in histopathology of joint tissues. Osteoarthr Cartil 2010;18:S113–6.
[52] Hu Q, Ecker M. Overview of MMP-13 as a promising target for the treatment of osteoarthritis. Int J Mol Sci 2021;22(4):1742.
[53] Jean-Gilles D, Li L, Vaidyanathan V, King R, Cho B, Worthen DR, et al. Inhibitory effects of polyphenol punicalagin on type-II collagen degradation in vitro and inflammation in vivo. Chem Biol Interact 2013;205(2):90–9.
[54] Vincenti MP, Brinckerhoff CE. Transcriptional regulation of collagenase (MMP-1, MMP-13) genes in arthritis: integration of complex signaling pathways for the recruitment of gene-specific transcription factors. Arthritis Res Ther 2002;4(3):157.
[55] Zhang M, Zhou Q, Liang Q-Q, Li C-G, Holz J, Tang D, et al. IGF-1 regulation of type II collagen and MMP-13 expression in rat endplate chondrocytes via distinct signaling pathways. Osteoarthr Cartil 2009;17(1):100–6.
[56] Linus A, Tanska P, Nippolainen E, Tiitu V, Töyras J, Korhonen RK, et al. Site-specific elastic and viscoelastic biomechanical properties of healthy and osteoarthritic human knee joint articular cartilage. J Biomech 2024;169:112135.
[57] Mäkelä J, Rezaeian Z, Mikkonen S, Madden R, Han S-K, Jurvelin J, et al. Site-dependent changes in structure and function of lapine articular cartilage 4 weeks after anterior cruciate ligament transection. Osteoarthr Cartil 2014;22(6):869–78.
[58] Desrochers J, Amrein M, Matyas J. Viscoelasticity of the articular cartilage surface in early osteoarthritis. Osteoarthr Cartil 2012;20(5):413–21.
[59] Lu X, Mow V, Guo X. Proteoglycans and mechanical behavior of condylar cartilage. J Dent Res 2009;88(3):244–8.
[60] Apte SS. Anti-ADAMTS5 monoclonal antibodies: implications for aggrecanase inhibition in osteoarthritis. Biochem J 2016;473(1):e1–4.
[61] Chen P, Zhu S, Wang Y, Mu Q, Wu Y, Xia Q, et al. The amelioration of cartilage degeneration by ADAMTS-5 inhibitor delivered in a hyaluronic acid hydrogel. Biomaterials 2014;35(9):2827–36.
[62] Julkunen P, Kiviranta P, Wilson W, Jurvelin JS, Korhonen RK. Characterization of articular cartilage by combining microscopic analysis with a fibril-reinforced finite-element model. J Biomech 2007;40(8):1862–70.
[63] Korhonen RK, Laasanen MS, Töyräs J, Lappalainen R, Helminen HJ, Jurvelin JS. Fibril reinforced poroelastic model predicts specifically mechanical behavior of normal, proteoglycan depleted and collagen degraded articular cartilage. J Biomech 2003;36(9):1373–9.
[64] Venäläinen MS, Mononen ME, Salo J, Räsänen LP, Jurvelin JS, Töyräs J, et al. Quantitative evaluation of the mechanical risks caused by focal cartilage defects in the knee. Sci Rep 2016;6(1):37538.
[65] Maldonado M, Nam J. The role of changes in extracellular matrix of cartilage in the presence of inflammation on the pathology of osteoarthritis. Biomed Res Int 2013;2013(1):284873.
[66] Rapp AE, Zaucke F. Cartilage extracellular matrix-derived matrikines in osteoarthritis. Am J Phys Cell Phys 2023;324(2):C377–94.
[67] Si Y, Tan Y, Gao L, Li R, Zhang C, Gao H, et al. Mechanical properties of cracked articular cartilage under uniaxial creep and cyclic tensile loading. J Biomech 2022;134:110988.
[68] Flachsmann R, Kistler M, Rentzios A, Broom N. Influence of an initiating microsplit on the resistance to compression-induced rupture of the articular surface. Connect Tissue Res 2006;47(2):77–84.
[69] Ebrahimi M, Turkiewicz A, Finnilä MAJ, Saarakkala S, Englund M, Korhonen RK, et al. Associations of human femoral condyle cartilage structure and composition with viscoelastic and constituent-specific material properties at different stages of osteoarthritis. J Biomech 2022;145:111390. doi: https://doi.org/10.1016/j.jbiomech.2022.111390.
[70] June RK, Fyhrie DP. Molecular NMR T2 values can predict cartilage stress-relaxation parameters. Biochem Biophys Res Commun 2008;377(1):57–61. doi: https://doi.org/10.1016/j.bbrc.2008.09.067.
[71] Han G, Eriten M, Henak CR. Rate-dependent crack nucleation in cartilage under microindentation. J Mech Behav Biomed Mater 2019;96:186–92.